Full Title: Transcriptome analysis indicates dominant effects on ribosome and mitochondrial function of a premature termination codon mutation in the zebrafish gene *psen2*

Short Title: Transcriptome analysis of a dominant *psen2* mutation in zebrafish

Authors: Haowei Jiang[1], Stephen Martin Pederson[2], Morgan Newman[1], Yang Dong[1], Michael Lardelli[1,*]

Affiliations: [1]University of Adelaide, School of Biological Sciences, Alzheimer's Disease Genetics Laboratory, North Terrace, Adelaide, SA 5005, AUSTRALIA

[2] University of Adelaide, School of Biological Sciences, Bioinformatics Hub, North Terrace, Adelaide, SA 5005, AUSTRALIA

***Corresponding Author:** Michael Lardelli, University of Adelaide, School of Biological Sciences, Alzheimer's Disease Genetics Laboratory, North Terrace, Adelaide, SA 5005, AUSTRALIA. Email: michael.lardelli@adelaide.edu.au

Key words: familial Alzheimer's disease, PRESENILIN 2, RNA-seq, zebrafish, mitochondrion

Abbreviations: ACRF, Australian Cancer Research Foundation; AD, Alzheimer's

Disease; Cas9, CRISPR associated protein 9; CPM, counts per million; CQN, continuous query notification; CRISPR, clustered regularly interspaced short palindromic repeats; DE, differentially expressed; DoLA, dorsal longitudinal ascending neuron; dNTPs, deoxynucleotide triphosphates; dqPCR, digital quantitative PCR; EGFP, enhanced green fluorescent protein; EOfAD, early onset familial Alzheimer's disease; ER, endoplasmic reticulum; F1/F2/F3, 1st/2nd/3rd filial generation; FC, fold change; FDR, false discovery rate; GO, Gene Ontology; GSEA, gene set enrichment analysis; Hom/HOM, homozygous; Het/HET, heterozygous; KEGG, Kyoto Encyclopedia of Genes and Genomes; MAM, mitochondria-associated membranes (of the ER); MAPK, MITOGEN-ACTIVATED PROTEIN KINASE; MD, mean difference; MsigDB, Molecular Signatures Database; NHEJ, non-homologous end joining; NMD, nonsense-mediated mRNA decay; ORF, open reading frame; PCR, polymerase chain reaction; PSEN1, PRESENILIN 1; PSEN2, PRESENILIN 2; rRNA, ribosomal RNA; sgRNA, single guide RNA; TM1, transmembrane domain 1; WT, wild type.

Financial Disclosure Statement: This research was supported by grants from the National Health and Medical Research Council of Australia, GNT1061006 and GNT1126422, and by funds from the School of Biological Sciences of the University of Adelaide. HJ was supported by an Adelaide Scholarship International scholarship from the University of Adelaide. YD is supported by an Adelaide Graduate Research Scholarship from the University of Adelaide.

45

46 **Conflict of Interest Statement:** The authors declare no conflict of interest.

Abstract

PRESENILIN 2 (*PSEN2*) is one of the genes mutated in early onset familial Alzheimer's disease (EOfAD). *PSEN2* shares significant amino acid sequence identity with another EOfAD-related gene *PRESENILIN 1* (*PSEN1*), and partial functional redundancy is seen between these two genes. However, the complete range of functions of *PSEN1* and *PSEN2* is not yet understood. In this study, we performed targeted mutagenesis of the zebrafish *psen2* gene to generate a premature termination codon close downstream of the translation start with the intention of creating a null mutation. Homozygotes for this mutation, $psen2^{S4Ter}$, are viable and fertile, and adults do not show any gross pigmentation defects, arguing against significant loss of γ-secretase activity. Also, assessment of the numbers of Dorsal Longitudinal Ascending (DoLA) interneurons that are responsive to *psen2* but not *psen1* activity during embryogenesis did not reveal decreased *psen2* function. Transcripts containing the *S4Ter* mutation show no evidence of destabilization by nonsense-mediated decay. Forced expression in zebrafish embryos of fusions of $psen2^{S4Ter}$ 5' mRNA sequences with sequence encoding enhanced green fluorescent protein (EGFP) indicated that the $psen2^{S4Ter}$ mutation permits utilization of cryptic, novel downstream translation start codons. These likely initiate translation of N-terminally truncated Psen2 proteins that obey the "reading frame preservation rule" of *PRESENILIN* EOfAD mutations. Transcriptome analysis of entire brains from a 6-month-old family of wild type, heterozygous and homozygous $psen2^{S4Ter}$ female siblings revealed profoundly dominant effects on gene expression likely indicating changes in ribosomal, mitochondrial, and anion transport functions.

Introduction

PRESENILIN 2 (*PSEN2*) was first identified as a candidate locus for mutations causing familial Alzheimer's disease (AD) with early onset (EOfAD) when a point mutation resulting in the substitution of an isoleucine residue for an asparagine residue (N141I) was found in a Volga German AD family in 1995 (1). *PSEN2* is similar in structure to the major EOfAD gene *PRESENILIN 1* (*PSEN1*) and the two genes encode proteins with 62% amino acid sequence identity (2). The age of onset of Alzheimer's disease (AD) caused by mutations in *PSEN2* ranges from 39 to 75 years, which overlaps both with *PSEN1* EOfAD-associated mutation disease onset ages and with late onset, sporadic AD (3). The later mean onset age of AD caused by *PSEN2* mutations compared to mutations in *PSEN1* is still unexplained, but some studies suggest that it may be caused by the partial replacement of *PSEN2* function by *PSEN1* (4). However, the functions of *PSEN1* and *PSEN2* have not yet been determined comprehensively. Moreover, despite the partial functional redundancy between *PSEN1* and *PSEN2*, *in vitro* studies have shown that the protein products of the two genes also play divergent roles in cellular physiology ((5, 6) and reviewed in (7)).

Both PSEN1 and PSEN2 proteins are components of γ-secretase complexes. The absence of PSEN1 is thought to reduce γ-secretase activity in mammalian cells (8, 9), while the absence of both PSEN1 and PSEN2 is thought to eliminate it completely (10, 11) although some data does not agree with this (reviewed in Jayne et al. (12)). In mice,

the loss of Psen1 causes premature differentiation of neural progenitor cells (NPC) and inhibition of Notch signaling leading to skeletal defects (13), and, ultimately, perinatal lethality (14). Mouse embryos lacking both Psen1 and Psen2 activity are more severely affected, showing earlier lethality and a developmental phenotype similar to loss of Notch1 activity (15, 16). However, by itself, the absence of Psen2 activity in mice does not appear to affect development significantly (17). In zebrafish, the inhibition of either Psen1 or Psen2 translation caused decreased melanocyte numbers in trunk and tail and other effects of decreased Notch signaling indicating a possibly greater role in Notch signaling for Psen2 protein in zebrafish compared to in mammals (18). Inhibition of Psen2 translation also led to increased Dorsal Longitudinal Ascending (DoLA) interneuron number, while inhibition of Psen1 translation showed no effect on this neuronal cell type (18).

Although mammalian *Psen1* and *Psen2* show compensatory regulation with forced down-regulation of one causing up-regulation of the other (19, 20), only *Psen2* down-regulation causes markedly decreased γ-secretase activity in the microglial cells of mice. The inhibition of γ-secretase activity caused by forced down-regulation of *Psen2* led to exaggerated proinflammatory cytokine release from microglia, indicating that *Psen2* plays an important role in central nervous system innate immunity (20). Furthermore, a negative regulator of monocyte pro-inflammatory response, miR146, was found to be constitutively down-regulated in the microglia of a *Psen2* knockout mouse strain, supporting that *Psen2* dysfunction may be involved in neurodegeneration through its

115 impacts on the pro-inflammatory behavior of microglia (21). Also, *Psen2* (but not
116 *Psen1*) knockout mice show reduced responsiveness to lipopolysaccharide as well as
117 decreased expression of nuclear factor kappa-light-chain-enhancer of activated B cells
118 (NF-kappaB), reduced mitogen-activated protein kinase (MAPK) activity and reduced
119 pro-inflammatory cytokine production. This indicates that *Psen2* has a specific
120 function(s) in innate immunity independent of *Psen1* (22).
121
122 The particular role of mammalian Psen2 protein in inflammation is consistent with its
123 restricted localization to the mitochondrial associated membranes (MAM) of the
124 endoplasmic reticulum (ER) (23). MAM formation has been shown to influence
125 inflammatory responses, is the site of autophagosome initiation, and plays a major role
126 in regulating mitochondrial activity (reviewed in Marchi et al (24)).
127
128 Considerable evidence supports roles for PRESENILIN proteins in the function of
129 mitochondria (25), which are central to energy production in cells and to other cellular
130 processes affected in AD such as apoptosis, reactive oxygen species production, and
131 calcium homeostasis (26). In human cell lines, it has been reported that PSEN2, but not
132 PSEN1, modulates the shuttling of Ca^{2+} between the ER and mitochondria since
133 mitochondrial Ca^{2+} dynamics are reduced by PSEN2 down-regulation and enhanced by
134 the expression of mutant forms of PSEN2 (27). In mouse cell lines, deficiency of *Psen2*
135 led to reduced expression of subunits responsible for mitochondrial oxidative
136 phosphorylation with altered morphology of the mitochondrial cristae, as well as an

137 increase in glycolytic flux. This indicated that absence of Psen2 protein causes an
138 impairment in respiratory capacity with a corresponding increase in glycolytic flux to
139 support cells' energy needs (28).
140
141 Despite the identification of hundreds of different EOfAD mutations in human *PSEN1*
142 and *PSEN2*, none of these appear to remove all gene function (i.e. none are null
143 mutations)(12). All *PRESENILIN* EOfAD mutations follow the "reading frame
144 preservation rule" meaning that they all produce at least one transcript variant
145 containing an open reading frame (ORF) termined by the original (non-mutant) stop
146 codon (12).
147
148 As part of an effort using zebrafish to identify the specific cellular changes caused by
149 EOfAD-like mutations in these genes, we wished to examine null mutations so that
150 their effects could be excluded from consideration. In this paper we describe an
151 unsuccessful attempt to generate a null mutation of the zebrafish orthologue of the
152 human *PSEN2* gene, *psen2*, by introduction of a premature termination codon
153 downstream of the asssumed translation start codon. Unexpectedly, the mutation
154 appears to force utilization of downsteam methionine codons for translation initiation.
155 This generates N-terminally truncated proteins that act dominantly in an EOfAD-like
156 manner.
157
158

Materials and Methods

Animal ethics

All experiments using zebrafish were conducted under the auspices of the Animal Ethics Committee of the University of Adelaide. Permits S-2014-108 and S-2017-073.

sgRNA design and synthesis

The target sequence of Ps2Ex3 sgRNA is 5'-CAGACAGTGAAGAGGAC *TCC*-3'. This target sequence was cloned into the plasmid pDR274 (Addgene plasmid # 42250) (29). The Ps2Ex3 pDR274 plasmid was linearized with *HindIII-HF*® (NEB, Ipswich, Massachusetts, USA, R3104S), and then used as a template for synthesis of Ps2Ex3 sgRNA with the MAXIscript™ T7 Transcription Kit (Ambion, Inc, Foster City, California, USA, AM1312).

Injection of zebrafish embryos

Tübingen (wild type embryos were generated by mass mating. Ps2Ex3 sgRNA (90 ng/μL final concentration) was first mixed with Cas9 nuclease (Invitrogen, Carlsbad, California, USA, B25640), and then incubated at 37°C for 15 min to maximize cleavage efficiency. 5-10 nL of the mixture was injected into zebrafish

181 embryos at the one-cell stage. The injected embryos were subsequently raised for
182 mutation screening.
183
184 **Mutation detection in G0 injected embryos using T7 Endonuclease I**
185
186 Mutation detection was based on the T7 Endonuclease I assay (30). Since mismatches,
187 small insertions or deletions generated through non-homologous end joining (NHEJ)
188 result in failure of base-pairing in heteroduplexes at mutation sites, T7 Endonuclease I
189 is able to recognize and cleave at the sites of these mutations.
190
191 To test whether the CRISPR/Cas9 system had functioned in the injected G0 embryos,
192 10 embryos were randomly selected from each injected batch and pooled together for
193 genomic DNA extraction at ~24 hours post fertilization (hpf). To extract the genomic
194 DNA, these 10 embryos were placed in 100 µL of 50 mM NaOH and then heated to
195 95°C for 15 min, and then 1/10th volume of 1 M Tris-HCl, pH 8.0 was added to each
196 sample to neutralize the basic solution after cooling to 4°C (31). A pair of primers (5'-
197 AGGCCACATCACGATACAC -3' and 5'-TGACCCGTTTGCTGTCTG-3') binding
198 to the flanking regions of the intended cleavage site was designed to amplify the test
199 region (~472 bp) through PCR. The PCR conditions for this amplification reaction were
200 95°C, 2 min; 31 cycles of [95°C, 30 s; 58°C, 30 s; 72°C, 30 s]; then 72°C, 5 min. The
201 PCR products were purified using the Wizard® SV Gel and PCR Clean-Up System
202 (Promega, Wisconsin, USA, A9281) and annealed (denaturation at 95°C for 5 min and

then slow cooling of the samples at the rate of -2°C/sec from 95°C to 85°C and then -0.1°C/sec from 85°C to 25°C for annealing of heteroduplexes) before addition of T7 Endonuclease I (NEB, Ipswich, Massachusetts, USA, M0302S). Heteroduplexes containing small mutations at the intended site should be cleaved into two fragments, ~313 bp (upstream) and ~159 bp (downstream).

When the T7 Endonuclease I assay on injected G0 embryos showed the presence of mutation at the target site, the remaining embryos from the same injection batch were raised for further mutation screening and breeding.

Mutation detection in adult G0 and F1 fish using T7 Endonuclease I and Sanger sequencing

When a G0 injected fish had grown to sufficient size (>2 cm in length, 2 to 3 months old), the tip of its tail (~2 mm in length) was biopsied (clipped) under Tricaine (1.68µg/mL) anesthesia for genomic DNA extraction. The clipped tail was placed in 100 µL of 50 mM NaOH and then heated to 95°C for 15 min to extract genomic DNA. The sample was then cooled to 4°C, and a 1/10th volume of 1 M Tris-HCl, pH 8.0 was then added to each sample to neutralize the basic solution (31). The same T7 Endonuclease I assay used previously for mutation detection in G0 embryos was then applied to the genomic DNA extracted from the G0 adult fish biopsy. However, since each G0 mutation-carrying fish was probably mosaic for several different mutations at

the target site, each G0 fish was outbred to a wild type Tübingen fish, to produce the F1 progeny, some of which could be heterozygous for single mutations. The F1 fish were biopsied and screened using the T7 Endonuclease I assay when large enough. For F1 fish found to carry mutations, the PCR-amplified fragments were sent to the Australian Genome Research Facility (AGRF, North Melbourne, VIC, Australia) for **S**anger sequencing to identify the mutations.

An 8-bp deletion resulting in a frameshift downstream of the start codon of *psen2*, *psen2*^{S4Ter} (Figure 1), was identified. PCR primers specifically detecting this mutation were designed (*psen2*^{S4Ter} forward primer: 5'-TTCATGAATACCTGAAGAGG-3', wild type forward primer: 5'- TTCATGAATACCTCAGACAGTG-3', and reverse primer: 5'-GAACAGAGAATGTACTGGCAGC-3') for further screening. The PCR conditions for *psen2*^{S4Ter} mutant detection are 95°C, 2 min; 31 cycles of [95°C, 30 s; 55°C, 30 s; and then 72°C, 30 s]; 72°C, 5 min. The length of PCR products is ~230 bp. The PCR conditions for wild type-specific detection are 95°C, 2 min; 31 cycles of [95°C, 30 s; 60°C, 30 s; and 72°C 30 s]; 72°C, 5 min and the anticipated length of the PCR products is ~230 bp.

Figure 1. Predicted protein sequence of *psen2*^{S4Ter}. An 8-bp deletion resulted in a frameshift downstream of the nominal translation start codon of *psen2* creating a stop codon as the 4th codon.

247

248

249 **Breeding of *psen2*^{S4Ter} mutant fish**

250 The initial F1 fish carrying the *psen2*^{S4Ter} mutation was outbred to a wild type fish to
251 generate a population of F2 progeny that was 50% heterozygous mutants and 50% wild
252 type fish. Two F2 heterozygous mutant fish were then inbred to generate a family of F3
253 fish consisting of (theoretically) 50% heterozygous mutants, 25% homozygous mutants
254 and 25% wild type fish. This F3 family was raised to six months of age before brain
255 removal and total brain RNA extraction for RNA-seq and other analyses.

256

257 **Total RNA extraction from 6-month-old zebrafish brains**

258 Individual fish were genotyped using PCR. Fish of the desired genotype were then
259 selected and euthanized by sudden immersion in an ice water slurry for at least 30
260 seconds before immediate decapitation. The entire brain was then removed from the
261 cranium for extraction of total RNA for either digital quantitative PCR (dqPCR) on
262 cDNA or RNA-seq (below).

263

264 For dqPCR tests, six wild type, six heterozygous and six homozygous fish from the F3
265 family were selected. Three of each genotype were then exposed to acute hypoxia
266 (dissolved oxygen content of the water was ~1.0 mg/L) for ~2.5 h, while the remaining
267 three of each genotype were exposed to normoxia. Fish were then euthanized and brains
268 removed (as above) for total RNA was extracted using the RNeasy Mini Kit (QIAGEN,

Venlo, Netherlands, 74104). cDNA was synthesised from brain RNAs using the SuperScript™ III First-Strand Synthesis System (Invitrogen, Carlsbad, California, USA, 18080051) with Random Primers (Promega, Madison, Wisconsin, USA, C1181).

For RNA-seq, four wild type, four *psen2*^{S4Ter} heterozygous and four *psen2*^{S4Ter} homozygous mutant brains (all from female fish) were extracted from the same family. Total RNA from these brains was extracted using the *mir*Vana™ miRNA Isolation Kit (Ambion, Inc, Foster City, California, USA, AM1560). RNA samples were sent to the Australian Cancer Research Foundation (ACRF) Cancer Genomics Facility, Adelaide SA, Australia for sequencing.

Allele specific transcript expression analysis by dqPCR

Primers for dqPCR, including a reverse primer specifically detecting the wild type allele (5'-TCGTTGTAGGAGTCCTCTTCACTG-3'), a reverse primer specifically detecting the *psen2*^{S4Ter} allele (5'-TCGTTGTAGGAGTCCTCTTCAGG-3') and a common forward primer (5'-TTCCTCACTGAATTGGCGATG-3'), were designed for allele specific expression analysis of the F3 family using the QuantStudio™ 3D Digital PCR System (Life Sciences, Waltham, MA, USA) with the QuantStudio™ 3D Digital PCR 20K Chip Kit v2 and Master Mix (Life Sciences, Waltham, MA, USA, A26317) and SYBR™ Green I Nucleic Acid Gel Stain (Life Sciences, Waltham, MA, USA, S7563). The dqPCR conditions for assays of mutant allele or wild type allele expression were 96°C, 10 min; 49 cycles of [62°C, 2 min; 98°C, 30 s]; 62°C, 2 min. The lengths of the

anticipated PCR products are ~130 bp. 25 ng of total cDNA* from a sample was loaded into one chip for the dqPCR. The chips were read using QuantStudio™ 3D AnalysisSuite Cloud Software (Life Sciences, Waltham, MA, USA).

*Stated cDNA concentrations are based on measured concentrations of RNA under the assumption that subsequent reverse transcription is completely efficient.

Testing for aberrant *psen2* transcript splicing due to the *S4Ter* mutation

Fifteen 24-hour-old zebrafish embryos were collected into one tube. Total RNA was extracted using the QIAGEN RNeasy mini Kit (QIAGEN, Hilden, Germany). 400ng of total RNA from each brain was then used to synthesize 20µL of first-strand cDNA by reverse transcription (SuperScript III kit, Invitrogen, Camarillo, California, USA). 40ng of each cDNA preparation (a quantity calculated from the RNA concentration on the assumption that reverse transcription of RNA into cDNA was complete) was used to perform PCR using GoTaq® DNA polymerase (Promega, Madison, USA). Each 25µL PCR reaction contained 0.2mM of deoxyribonucleotide triphosphates (dNTPs), 0.4µM of each PCR primer, 1 unit of GoTaq® DNA polymerase and 40ng of zebrafish embryo cDNA template. PCR cycling was performed with 35 cycles of a denaturation temperature of 95°C for 30s, then an annealing temperature of 60°C for 45s and then an extension temperature of 72°C for 1.5 minutes. PCR products were electrophoresed through a 1.5% agarose gel in 1×TAE buffer for separation and identification. **PCR primers:** 5'UTR_F: 5'-TTTTGACGGAGTATTTTCGCAT-3', Exon3_F: 5'-

313 CTCTTCATCCCTGTCACGCTCT-3', Exon3_R: 5'-

314 CTCGGTGTAGAAACTGACGGACTT-3', Exon7_R: 5'-

315 TTCCACCAGCATCCTCAACG-3'.

316 **Construction of the *psen2* EGFP fusion expression vectors**

317 DNA sequence corresponding to the 5'UTR and the first 113 codons of the *psen2* gene
318 fused to sequence encoding the N-terminal end of EGFP (but excluding EGFP's
319 translation start codon) was synthesized by Integrated DNA Technologies Inc.
320 Coralville, Iowa, USA) and ligated into the pcGlobin2 vector between the *BamH* I and
321 *EcoR* I restriction sites to construct expression vector psen2WT-EGFP. The same
322 procedure was followed to construct expression vector psen2S4Ter-EGFP that is
323 identical to psen2WT-EGFP except that psen2S4Ter-EGFP lacks the 8 nucleotides
324 deleted in the $psen2^{S4Ter}$ mutant allele (i.e. 5'- CAGACAGT -3'). The complete
325 sequences of these fusion genes are given in supplementary data file S1 Appendix 1.

326

327 ***In-vitro* mRNA transcription and microinjection**

328 The psen2WT-EGFP and psen2S4Ter-EGFP expression vector constructs were
329 restricted with *Xba*I before transcription using the mMessage mMachine T7 kit
330 (Thermo Fisher Scientific Inc, Waltham, Massachusetts, USA) to generate mRNA. All
331 mRNAs were precipitated with LiCl and then redissolved in water for injection of 2-5
332 nL at a concentration of 400 ng/μL. No obvious developmental abnormalities were seen
333 after injection of these mRNAs into zebrafish embryos. At ~24 hpf, both the psen2WT-
334 EGFP mRNA- and the psen2S4Ter-EGFP mRNA-injected embryos showed weak

335 EGFP fluorescence (as visualized by fluorescence microscopy). For mRNA injected
336 and non-injected embryos (as negative controls) 15 embryos were collected for
337 subsequent western immunoblot analysis.
338
339 **Western immunoblot analyses**
340 Embryos at 24 hpf were first dechorionated and their yolks were removed in embryo
341 medium containing Tricaine methanesulfonate. Embryos were then placed in RIPA
342 extraction buffer (Sigma-Aldrich Corp. St. Louis, Missouri, USA) containing Complete
343 Proteinase Inhibitor (Sigma-Aldrich), homogenized and incubated at 4°C (with
344 rotation). Cell debris was sedimented from the protein sample by centrifugation at
345 16,000 x g for 30 seconds, LDS sample buffer (Invitrogen) was added to the supernatant,
346 the protein sample was heated at 80°C for 20 minutes and then stored at -80°C. Sample
347 Reducing Agent (Thermo Fisher Scientific) was added to samples prior to being loaded
348 onto NuPAGE™ 4-12% Bis-Tris Protein Gels (Invitrogen). The separated proteins
349 were subsequently transferred to a PVDF membrane (Bio-Rad Laboratories, Hercules,
350 California, USA) using the Mini Gel Tank and Blot Module Set (Thermo Fisher
351 Scientific). For EGFP protein detection, the PVDF membrane was blocked with
352 blocking reagent (Roche Holding AG, Basel, Switzerland) and then probed with the
353 primary antibody, polyclonal anti-GFP goat (Rockland Immunochemicals Inc.,
354 Gilbertsville, Pennsylvania, USA), followed by secondary antibody, horseradish
355 peroxidase (HRP) conjugated anti-goat antibody (Rockland). For subsequent beta-
356 tubulin (protein loading control) detection, the PVDF membrane was blocked in 5%

skim milk and then probed with the primary antibody, monoclonal beta-tubulin (E7, DSHB) followed by secondary antibody, horseradish peroxidase conjugated anti-mouse antibody (Rockland). Bound antibody was detected by chemiluminescence using SuperSignal™ West Pico PLUS Chemiluminescent Substrate (Thermo Fisher Scientific) and imaged by the ChemiDoc™ MP Imaging System (Bio-Rad Laboratories).

RNA-seq data generation and quality control

Paired-end (2x150bp) RNA Seq libraries were provided by the ACRF Cancer Genomics Facility. Briefly, RNA samples were depleted for rRNA using the methods of Adiconis (32) and sequences derived from mammalian rRNA, before being prepared using the KAPA Hyper RNA Library Prep kit (Roche Holding AG), and sequenced on an Illumina NextSeq 500 (Illumina, San Diego, California, USA). Libraries were generated for $n = 4$ samples from each of the genotypes: wild type (WT, *psen2*$^{+/+}$), heterozygous (Het, *psen2*^{S4Ter}/+) and homozygous (Hom, *psen2*^{S4Ter}/*psen2*^{S4Ter}), ranging in size from 27,979,654 to 37,144,975 reads. Libraries were trimmed using cutadapt v1.14 to remove Illumina Adapter sequences. Bases with a PHRED score < 30 were also removed along with NextSeq-induced polyG runs. Reads shorter than 35bp after trimming were discarded. Trimmed reads were aligned to GRCz11 using STAR v2.7.0 (33), and gene descriptions based on Ensembl release 98. For the purposes of genotype confirmation, trimmed reads were additionally aligned using kallisto

v0.43.1 (34) to a modified version of the Ensembl transcriptome, where the sequence for the psen2S4Ter allele was additionally included. RNA-seq data has been deposited in the Gene Expression Omnibus database (GEO) under Accession Number GSE148468.

Differentially expressed gene analysis of RNA-seq data

Unique alignments corresponding to strictly exonic regions from gene models in Ensembl release 98 were counted using featureCounts from the Subread package v1.5.2 (35), giving total counts per sample which ranged between 11,852,141 and 16,997,219. Genes with counts per million (CPM) > 1.5 in at least four samples were retained, whilst genes whose biotype corresponded to any type of rRNA were additionally excluded, giving 16,640 genes for differential expression analysis. As GC bias was suspected, given variable rRNA depletion across samples, gene-level counts were normalized for GC and length bias using CQN (36), before estimating fold change using the GLM likelihood-ratio test in the R package edgeR (37). Differential expression was determined for the presence of the mutant allele and the comparison between heterozygous and homozygous mutants. P-values from likelihood-ratio tests were adjusted using both the Benjamini-Hochberg FDR procedure, and the Bonferroni adjustment to provide two complementary view points on the data. Genes were considered to be differentially expressed in the presence of a mutant allele if satisfying one of two criteria, either 1) a Bonferroni-adjusted p-value < 0.01, or 2) an FDR-adjusted p-value < 0.01 along with a logFC estimate beyond the range $\pm$ 1. For the

401 comparison between mutant genotypes, genes were considered to be exhibiting
402 differential expression if obtaining an FDR-adjusted p-value < 0.05 in this comparison.
403 Code for the complete analysis is available at
404 https://uofabioinformaticshub.github.io/20170327_Psen2S4Ter_RNASeq/
405
406 **Genotype confirmation in RNA-seq data**
407 Genotypes were confirmed for each RNASeq sample using transcript-level counts for
408 the *psen2* wild-type allele and the *psen2*^{S4Ter} allele. No expression of the WT allele was
409 overserved in any homozygous mutant, whilst no expression of the mutant allele was
410 observed in homozygous WT samples. A ratio of approximately 1:1 between mutant
411 and WT alleles was observed in all heterozygous mutant samples, as expected.
412
413 **Enrichment analysis**
414 Enrichment testing was performed using Hallmark, KEGG and GO genesets from the
415 MSigDB database (38), with GO terms excluded if the shortest path back to the root
416 node was < 3 steps. For the comparison between mutant and wild-type samples,
417 enrichment analysis was performed on the set of 615 DE genes using goseq (39), setting
418 gene-level correlation with sample-specific rRNA content as a covariate. For the
419 comparison between mutant genotypes, the number of DE genes was considered to be
420 too small for this type of analysis. An additional enrichment analysis on the complete
421 dataset was performed using fry on comparisons both between mutant and wild-type,
422 and between mutant genotypes, as fry more appropriately handles inter-gene

correlations than approaches like GSEA (40).

In situ transcript hybridization analysis of DoLA neuron number

This was performed as previously described (41) on embryos from a pair mating of two *S4Ter* heterozygous mutants. After counting of DoLA neurons in an embryo, the embryo was subjected to DNA extraction as for the tail biopsies (above) and then its *psen2* genotype was determined by allele-specific PCRs.

Results

Generation of a putatively null mutation in zebrafish *psen2*

As part of a program analyzing the function of genes involved in familial Alzheimer's disease, we wished to identify changes in the expression of genes in adult brains due to simple loss of *PSEN2* activity. We previously identified the *psen2* gene in zebrafish (42) and the ENSEMBL database (http://asia.ensembl.org) reports one *psen2* transcript (ENSDART00000006381.7) with 11 exons and the translation start codon residing in exon 2. Therefore, we used the CRISPR Cas9 system to generate a frameshift mutation just downstream of this transcript's nominal translation start codon (intended to allow ribosomes to initiate translation but not translate Psen2 protein). A frameshift mutation (a deletion of 8 nucleotides) starting in the 4th codon and resulting in the creation of a translation termination codon was isolated (Figure 1). The mutant allele is designated *psen2*^{S4Ter}.

No decreased stability of mutant allele transcripts under normoxia or hypoxia

Premature termination codons in transcripts frequently cause nonsense-mediated decay when more than 50-55 nucleotides upstream of an exon-exon boundary (43). Also, hypoxia appears to be an important element in AD (44, 45) and increases the expression of *PSEN* gene transcripts in both human and zebrafish cells (46, 47). Therefore, we sought to determine whether transcripts of the *psen2*^{S4Ter} allele are less stable than wild type transcripts and to observe the expression of mutant allele transcripts under acute hypoxia. We used dqPCR with allele-specific primer pairs to quantify relative transcript numbers in cDNA synthesized from the brains of 6-month-old wild type, heterozygous and homozygous mutant fish under normoxia or acute hypoxia (see Materials and Methods). The results of this analysis are shown in Figure 2. In heterozygous fish under normoxia, both wild type and mutant allele transcripts are expressed at similar levels in 6-month-old brains, with the wild type allele expressed at approximately half the level seen in wild type fish (i.e. that possess two wild type alleles). As expected, acute hypoxia increases the expression of the wild type transcript and this is also observed for the mutant transcript that shows no evidence of destablization (Figure 2).

Figure 2. Allele-specific mRNA expression in the brains of 6-month-old fish of different genotypes under normoxia or acute hypoxia (as copies per 25 ng of brain cDNA in each digital qPCR) (A) The levels of wild type *psen2* allele mRNA in the

467 *psen2*^{S4Ter}/+ fish (~700 copies) were significantly (p=0.0115) lower than in their wild
468 type siblings (~1,300 copies) under normoxia. Under hypoxia, the levels of wild type
469 *psen2* allele mRNA in both the *psen2*^{S4Ter}/+ fish (~1,000 copies) and their wild type
470 siblings (~1,800 copies) were up-regulated, but only the higher levels in the wild type
471 fish showed a statistically significant increase (p=0.0313) compared to the normoxic
472 controls. (B) The levels of *psen2*^{S4Ter} allele mRNA in the *psen2*^{S4Ter}/+ fish (~700 copies)
473 were significantly (p=0.0498) lower than in the *psen2*^{S4Ter}/*psen2*^{S4Ter} fish (~1,000 copies)
474 under normoxia. Under hypoxia, the levels of *psen2*^{S4Ter} allele mRNA in both the
475 *psen2*^{S4Ter}/+ fish (~1,000 copies) and the *psen2*^{S4Ter}/*psen2*^{S4Ter} fish (~1,900 copies) were
476 upregulated. This up-regulation in the *psen2*^{S4Ter}/*psen2*^{S4Ter} fish was clearly significant
477 (p=0.0049), while that in the *psen2*^{S4Ter}/+ fish was apparent, but not regarded as
478 statistically significant (p=0.0837). The dqPCR raw data is given in supplementary data
479 file S1 Table 1 & 2.
480
481 ---
482
483 **No increase in DoLA neuron number in embryos homozygous for *S4Ter***
484 Currently, we do not have an antibody against zebrafish Psen2 protein that would allow
485 us to demonstrate loss of Psen2 activity in homozygous mutants. Also concerning is
486 that a frameshift allele of *psen2* that we have isolated separately, *N140fs*, shows loss of
487 surface melanotic pigmentation when homozygous, suggesting loss of γ-secretase
488 activity (48) whereas homozygous *S4Ter* mutants do not. Therefore, we sought an

alternative method to demonstrate loss of *psen2* function due to the *S4Ter* mutation.

Inhibition of *psen2* mRNA translation has been shown to increase the number of a particular spinal cord interneuron – the Dorsal Longitudinal Ascending (DoLA) neuron in zebrafish embryos at 24 hours post fertilization (hpf) (41). Therefore, if *S4Ter* decreases *psen2* function, it might be expected to increase DoLA number (although, as an endogenous mutation rather than blockage of gene expression using a morpholino, *S4Ter* might induce genetic compensation to suppress this phenotype (49)). To examine the effect of *S4Ter* on DoLA number, we collected embryos from a pair-mating of two *psen2*^{S4Ter}/+ fish to generate a family of embryos comprised, theoretically, of 50% heterozygous mutants, 25% homozygous mutants and 25% wild type genotypes. The embryos were allowed to develop to the 24 hpf stage before *in situ* transcript hybridization against transcripts of the gene *tbx16* that labels DoLA neurons (50). After the number of DoLA neurons in each embryo had been recorded, each embryo was genotyped using PCRs specific for the mutant and wild type alleles. Two-tailed t-tests found no significant differences in DoLA number between any two genotypes. This does not support that *S4Ter* reduces *psen2* activity (Figure 3). Nevertheless, transcriptome analysis (below) shows distinct differences between the brain transcriptomes of *S4Ter* mutant and wild type siblings.

---

511 **Figure 3. DoLA neuron number assessment of *psen2* activity.** 42 embryos at 24 hpf
512 from a pair-mating of a *psen2*^{S4Ter}/+ female and a *psen2*^{S4Ter}/+ male were subjected to
513 *in situ* hybridization to detect DoLA neurons that were then counted. Subsequent
514 genotyping of individual embryos revealed 21 heterozygous mutants, 16 homozygous
515 mutants and 5 wild type embryos. Values of p were determined in two-tailed t-tests.
516 Raw data is given in supplementary data file S1 Table 3.

517

518 ---

519

520 **No apparent effects of the *S4Ter* mutation on transcript splicing**

521 The retention of melanotic pigmentation and normal DoLA neuron number in S4Ter
522 homozygous fish implied that this mutant allele still produces a functional protein. To
523 understand how this might occur, we first checked to see whether the mutation
524 influenced transcript splicing. The *psen2* translation initiation codon and the S4Ter
525 mutation both exist in the second exon of the gene. To test for changes in transcript
526 splicing, we generated cDNA using total RNA purified from wild type and S4Ter
527 homozygous embryos at 24 hours post fertilization (hpf). We then performed PCR
528 using primer pairs binding to sequences in exons 1 and 3, 3 and 7, and 1 and 7 (See
529 Materials and Methods and supplementary data file S1 Appendix 2). Each PCR
530 amplified a single cDNA fragment of the expected size that was essentially identical
531 between the wild type and mutant larvae. (Size differences due to the deletion of 8
532 nucleotides in the S4Ter mutant allele could not be resolved). Therefore, there is no

533 evidence that the S4Ter mutation changes the splicing of nascent *psen2* transcripts.

534

535 **The *S4Ter* mutation allows downstream Met codons to initiate translation**

536 The *S4Ter* mutation might still allow production of a functional protein if a downstream
537 Met codon could act to initiate translation, and the resultant protein retained γ-secretase
538 catalytic activity. Three Met codons exist in the N-terminal-encoding region of the
539 *psen1* ORF (Figure 4A); codons 34, 88, and 97. Codon 34 exists in the cytosolic-coding
540 region before the first transmembrane domain (TM1), while codon 88 codes for a Met
541 residue near the cytosolic surface of TM1 and codon 97's Met residue is deep within
542 TM1. Since the transmembrane domains of PRESENILIN proteins show high sequence
543 conservation during evolution, we assumed that a protein lacking TM1 could not
544 function so that a functional Psen2 protein might only form if codon 34 or 88 (and
545 remotely possibly 97) were used to initiate translation. Therefore, we fused the known
546 5'UTR sequences and the first 113 codons of the *psen2* ORF (that includes codons for
547 all TM1 residues) to sequence coding for enhanced green fluorescent protein (EGFP,
548 excluding the EGFP start codon) and incorporated this into the vector pcGlobin2 for
549 synthesis of mRNA. Both wild type and *S4Ter*-mutant versions of this construct were
550 produced (see Figure 4A). Synthetic mRNAs from these vectors were injected into
551 zebrafish embryos at the 1-cell stage and western immunoblots of 24 hpf embryos were
552 subsequently probed with an antibody detecting GFP. This revealed the expected
553 translation initiation from the wild type sequence predominantly at codon 1 (Figure
554 4B). However, in the presence of the *S4Ter* mutation, there was apparent translation

initiation at codon 34 and at either one or both of codons 88 and 97 (although the western immunoblot lacked the resolution to distinguish which, Figure 4B). Therefore, it is highly likely that the *S4Ter* mutant allele produces one or more forms of N-terminally truncated Psen2 protein. Interestingly, these would obey the reading frame preservation rule of the *PRESENILIN* EOfAD mutations and so might reasonably be expected to produce dominant, EOfAD-like effects on brain transcriptomes.

Figure 4. Testing for translation initiation at novel downstream start codons. A. The constructs used to test for translation initiation at Met codons downstream of the S4Ter mutation. S1 represents the wild type translation start site and S2-4 are potential downstream translation initiation sites within the first 113 codons. **B.** Western immunoblotting of lysates from embryos injected with the constructs described in A. Translation initiation at S1 (S1-EGFP) does not permit initiation at S2-4. However, in the presence of the S4Ter mutation, initiation is evident at S2 (S2-EGFP) and either S3 or S4 or both (S3/4-EGFP). The identity of the low intensity ~35kDa protein band is not known but it may be a degradation product of larger fusion protein species. Free EGFP can be produced from EGFP fusion protein species in the lysosome (51, 52).

Large zebrafish families facilitate reduction of genetic and environmental noise

577 An advantage of genetic analysis in zebrafish is the ability to reduce genetic and
578 environmental variation in statistical analyses through breeding of large families of
579 siblings that are then raised under near identical environmental conditions (i.e. in the
580 same fish tank or recirculated water aquarium system). The initial heterozygous
581 individual fish identified as carrying *psen2*^{S4Ter} was outbred to a wild type fish of the
582 same strain (Tübingen) and then two heterozygous individuals were mated to produce
583 a large family of siblings with wild type (+/+), heterozygous (*psen2*^{S4Ter}/+), or
584 homozygous (*psen2*^{S4Ter}/ *psen2*^{S4Ter}) genotypes. (We have subsequently established a
585 line of fish homozygous for the *psen2*^{S4Ter} mutant allele, demonstrating that these fish
586 are both viable and fertile.)
587
588 Laboratory zebrafish become sexually mature at between 3 and 5 months of age.
589 Therefore, to examine the transcriptome of young adult zebrafish brains we identified
590 individuals of the desired genotype using PCRs specific for the mutant and wild type
591 alleles on DNA from tail biopsies ("tail clips") and then removed brains from fish of
592 the desired genotypes at 6 months of age. Total RNA was then purified from these and
593 subjected to either RNA-seq analysis (described below) or digital quantitative PCR
594 (dqPCR) as shown previously in Figure 2).
595
596 **RNA-seq data and analysis of *psen2*^{S4Ter} effects**
597 To analyze and compare the brain transcriptomes of 6-month-old wild type,
598 heterozygous and homozygous mutant siblings, four female fish of each genotype were

599 examined (Figure 5A). An exploratory principal component analysis (PCA) of gene
600 expression across all samples was generated using gene-level, $\log_2$-transformed counts
601 per million (Figure 5B), indicating that the difference between wild type (+/+) samples
602 and mutant samples was the dominant source of variability, with PC1 (30.9% of
603 variance) clearly separating the homozygous (Hom) and heterozygous (Het) mutant fish
604 brains from those of the wild type (WT) fish. The Hom and Het mutant fish were largely
605 overlapping with respect to both PC1 and PC2, with the latter accounting for 15.2% of
606 variance in the total dataset.

607 ---

608

609 **Figure 5. Brain transcriptome analysis A**. Pair-mating of two Het zebrafish produces
610 a family made up of WT, Het, and Hom siblings in a ~1:2:1 ratio respectively. At six
611 months of age, the transcriptomes of entire brains from four female sibling fish each of
612 WT, Het, and Hom genotypes were analyzed. **B.** PCA analysis showing PC1 and PC2
613 using logCPM values from each sample. The largest source of variability within this
614 dataset was clearly the difference between wild type samples and those containing one
615 or two copies of the *psen2*^{S4Ter} allele. **C**. Volcano plots displaying gene differential
616 expression (DE) p-values versus fold-change. Left: DE genes from comparison of Het
617 and Hom brains. Right: DE genes from comparison of brains of fish possessing the
618 *S4Ter* allele (i.e. either Het or Hom) versus WT. The dominant nature of the *S4Ter*
619 mutation is indicated by the relatively restricted differences between Het and Hom
620 transcriptomes compared to *S4Ter* vs. WT.

621

622

---

623 **Differentially expressed genes (DE genes)**

624

625 As the Heterozygous and Homozygous *psen2*^{S4Te} brains showed very similar patterns
626 of gene expression, we fitted a statistical model for the presence of the mutant allele
627 with an additional term to capture the difference between the two mutant genotypes
628 (Figure 5). In the analysis based on the presence of the mutant allele, genes were
629 considered to be DE using either 1) A Bonferroni-adjusted p-value < 0.01 or, 2) An
630 FDR-adjusted p-value < 0.01 along with an estimated logFC outside of the range ±1.
631 However, as far fewer DE genes were detected when comparing brain transcriptomes
632 between mutant genotypes, a simple FDR of 0.05 was chosen as the DE criterion for
633 that comparison (see supplementary data file S2 Sheet 1 & 3). Ultimately, 615 genes
634 were declared to be DE due to any presence of the *psen2*^{S4Ter} mutant allele, while 7
635 genes were declared to be DE between brains with Hom and Het genotypes. Heatmaps
636 (Figure 6) for the most highly ranked (by FDR) of these DE genes show that the DE
637 genes cluster according to genotype as expected.

638

639

640 **Figure 6. Heatmaps of DE genes**. Plotted values are logCPM based on CQN-
641 normalized counts. **A**. The most highly ranked 40 (of the 615) DE genes by FDR
642 identified when comparing WT fish to genotypes possessing the *psen2*^{S4Ter} allele. **B**.

643 The 7 most highly-ranked genes (FDR < 0.05) which were detected as DE between Het
644 and Hom mutant genotypes. Unique sample name identifiers are given beneath each
645 column.

646 _____

647

648 **Results from Enrichment Analyses**

649 To predict what changes in molecular/cellular processes might be reflected by the
650 differential expression of genes, enrichment analyses were conducted using the
651 Hallmark, KEGG and GO gene sets defined in the MSigDB database (38). A detailed
652 description of the analyses is publicly available at:
653 https://uofabioinformaticshub.github.io/20170327_Psen2S4Ter_RNASeq/
654 Full results of enrichment analyses are also listed in supplementary data file S2 sheet 2
655 & 4. Overall, two strategies for enrichment analysis were used: 1) Testing for
656 enrichment within *discrete sets of DE genes* (WT versus presence of *psen2*^{S4Ter} only).
657 2) Testing for enrichment within the *complete gene lists*, i.e. regardless of DE status,
658 but using direction of fold-change and p-values as a ranking statistic.).

659

660 During analysis, we found that the RNA-seq data indicated considerable (and variable)
661 ribosomal RNA (rRNA) content, presumably due to somewhat inefficient depletion of
662 zebrafish rRNA from samples, using a human genome-based rRNA depletion kit. While
663 rRNA sequences could be excluded from the subsequent RNA-seq data
664 bioinformatically, the primary enrichment within DE genes indicated pathways such as

KEGG_RIBOSOME and *CYTOSOLIC_RIBOSOME* raised concerns that the rRNA contamination might somehow have biased the sampling of cellular RNA, although a mechanism for this is not immediately obvious. Our caution was also raised by recent work showing that gene length might bias the detection of DE gene transcripts in RNA-seq datasets (53). In particular, as a set, ribosomal protein genes have short lengths and may be prone to artefactual identification as DE due to this bias (53). However, when examining the complete gene lists using fry, additional terms which were clearly distinct to rRNA became evident, such as *OXIDATIVE PHOSPHORYLATION* (dre00190), *MITOCHONDRIAL ENVELOPE* (GO:0005740) and *ANION TRANSPORT* (GO:0006820) (Figure 7). As these terms shared virtually no genes with ribosomal-related gene sets, this increases our confidence that these represent real biological differences that are affected by the presence of the *psen2*^{S4Ter} allele.

Figure 7. UpSet plot indicating distribution of DE genes within larger significant terms from the GO gene sets. For this visualization, GO terms were restricted to those with 15 or more DE genes, where this represented more than 5% of the gene set, along with an FDR < 0.02 and more than 3 steps back to the ontology root. The 20 largest GO terms satisfying these criteria are shown with the plot being truncated at the right hand side for simplicity. A group of 28 genes is uniquely attributed to the GO *MITOCHONDRIAL ENVELOPE* (orange shading), with a further 18 being relatively unique to the GO *MRNA METABOLIC PROCESS*. The next grouping of 15

687 genes is unique to GO *REGULATION OF NUCLEOBASE-CONTAINING*
688 *COMPOUND METABOLIC PROCESS* followed by 25 genes, spread across two
689 clusters of terms which largely represent GO *RIBOSOMAL ACTIVITY*. In between
690 these are 13 genes uniquely associated with the GO *ANION TRANSPORT*.
691 _____
692
693 The presence of the *psen2*^{S4Ter} mutation was predicted to affect a number of metabolic
694 pathways, particularly Xenobiotic Metabolism (M5934) from the Hallmark gene sets.
695 However, pathways similar to those seen for an EOfAD-like mutation in the zebrafish
696 *psen1* gene (54), were also observed in the brains of fish with *psen2*^{S4Ter}, particularly
697 those involving energy production by mitochondria. When homozygous and
698 heterozygous *psen2*^{S4Ter} brains were compared, the pathways were even more closely
699 focused around oxidative phosphorylation and mitochondrial function, probably
700 reflecting a critical role for the Psen2 protein in regulating mitochondrial energy
701 production. All pathway enrichment data as generated under fry is given in S2 Sheet 2
702 & 4.
703
704

Discussion

Well over 200 mutations causing familial Alzheimer's disease have been identified in the human *PSEN1* and *PSEN2* genes. However, none of these mutations are obviously null (e.g. are frameshift or nonsense mutations that block all mRNAs from producing a protein that includes the normal C-terminal residues) (12). Knowledge of the molecular effects of null mutations in these genes is, therefore, useful since, by exclusion, it could help us determine the functions critically affected by EOfAD mutations.

Alzheimer's disease takes decades to develop, but we are unable to investigate in detail the molecular changes occurring in the brains of young human carriers of EOfAD mutations since biopsies cannot be taken. Consequently, analysis in animal models is necessary. In this study, we attempted to generate a null mutation in the zebrafish *psen2* gene. We identified an 8-bp deletion in the zebrafish *psen2* gene that forms a premature termination codon (PTC) at the fourth codon position downstream of the start codon (*psen2*^{S4Ter}). However, this PTC apparently fails to block translation and, instead, reveals cryptic downstream translation start codons that likely drive formation of N-terminally truncated Psen2 protein(s). One or more of these proteins apparently possesses γ-secretase activity since *psen2*^{S4Ter} homozygous fish possess melanotic surface pigmentation and normal DoLA neuron numbers in 24 hpf embryos. Translation initiation at cryptic downstream start codons would also explain the lack of NMD of *S4Ter* allele transcripts. The failure of NMD is unlikely to be due to the

proximity of the PTC to a downstream exon/exon splice boundary since the nearest such boundary would be far more than 55 nucleotides distant in a spliced mRNA (55).

The *psen2*^{S4Ter} allele shows dominance and may be EOfAD-like

Transcriptome analysis of 6-month-old entire brains from wild type, and *psen2*^{S4Ter} heterozygous and homozygous zebrafish showed relatively few differences between the heterozygous and homozygous fish centered around mitochondrial function while extensive changes from wild type were caused by any presence of the *psen2*^{S4Ter} allele. The differences that were seen between heterozygous and homozygous brains were in similar functions to those seen for any presence of *psen2*^{S4Ter} compared to wild type, only more extreme: effects on mitochondrial function (particularly oxidative phosphorylation) and ribosomal functions. This pattern of effects is most easily explained as *psen2*^{S4Ter} displaying a dominant negative phenotype. However, because homozygous fish retain melanotic skin pigmentation, we know that the protein produced by *psen2*^{S4Ter} retains some γ-secretase activity (48). Previous research on PRESENILIN protein function suggests two possibilities for the effects of *psen2*^{S4Ter} on mitochondria that are not mutually exclusive. In 2009, Area-Gomez et al (23) noted that, in mouse brain, PSEN2 protein is concentrated in the mitochondria-associated membranes of the ER, MAM. In later papers, these researchers noted that loss of *PSEN* gene activity causes increased association of ER membranes with mitochondria (i.e. increased MAM) (56) and decreased oxidative phosphorylation (oxygen consumption) in mouse embryonic fibroblasts (57). While the decreased oxidative phosphorylation

749 could be mimicked by chemical inhibition of γ-secretase, the extent of MAM formation
750 was less sensitive to γ-secretase activity. Increased MAM formation was also observed
751 in fibroblasts from people with EOfAD mutations in *PSEN2*, (or *PSEN1*, or with late
752 onset, sporadic AD) (56). Alternatively, in 2010, Lee et al (58) showed that the Psen1
753 holoprotein (i.e. not the endoproteolytically-cleaved, γ-secretase-active form of Psen1)
754 was required for normal acidification of lysosomes by promoting N-glycosylation of
755 the V0a1 subunit of v-ATPase that is required for its correct localization to the lysosome.
756 (Note that it has not yet been demonstrated formally that PSEN2 plays a similar role.)
757 Recently, Yambire et al. demonstrated that deficient lysosomal acidification can cause
758 insufficient importation of iron leading to mitochondrial dysfunction (59).
759
760 In a 2016 review, we suggested that mutant PRESENILIN holoproteins may interfere
761 with normal holoprotein (putative) multimerization and, thereby, act in a dominant
762 negative manner to interfere with the holoproteins' normal activity in promoting this
763 N-glycosylation event. (We suggested that the involvement of PRESENILIN
764 holoproteins in multimerization may explain the "reading frame preservation" rule that
765 states that all EOfAD mutations in the *PSEN* genes must preserve an open reading frame
766 that uses the original stop codon (12).) Curiously, both of the PRESENILIN activities
767 mentioned above, the regulation of MAM formation and of endolysosomal acidification,
768 appear to be mediated by the C99 fragment (β-CTF) of APP (57, 60) and this implies
769 that these activities of the PRESENILINs may share a common molecular mechanism.
770

771 In conclusion, the *psen2*^{S4Ter} mutation is not the null allele we had hoped to isolate and
772 probably results in production of N-terminally truncated Psen2 proteins. These
773 truncated proteins may act in an EOfAD-like manner through their conformity to the
774 "reading frame preservation rule" and display effects on mitochondrial function as we
775 previously observed for an EOfAD-like mutation of *psen1* (54). The *psen2*^{S4Ter} mutation
776 also appears to have significant effects on ribosomal functions although an unexpected
777 (and currently inexplicable) correlation of gene differential expression with degree of
778 rRNA contamination in brain RNA samples raises questions around the validity of this
779 result.
780

781 ## Acknowledgments

782 The authors wish to thank Seyyed Hani Moussavi Nik for kind assistance in adjusting
783 the conditions for the dqPCR.
784

785 # References

786

787 1. Levy-Lahad E, Wasco W, Poorkaj P, Romano DM, Oshima J, Pettingell WH, et al.
788 Candidate gene for the chromosome 1 familial Alzheimer's disease locus. Science.
789 1995;269(5226):973-7.
790 2. Newman M, Musgrave IF, Lardelli M. Alzheimer disease: amyloidogenesis, the
791 presenilins and animal models. Biochim Biophys Acta. 2007;3:285-97.
792 3. Ryman DC, Acosta-Baena N, Aisen PS, Bird T, Danek A, Fox NC, et al. Symptom
793 onset in autosomal dominant Alzheimer disease: a systematic review and meta-
794 analysis. Neurology. 2014;83(3):253-60.
795 4. Jayadev S, Leverenz JB, Steinbart E, Stahl J, Klunk W, Yu CE, et al. Alzheimer's
796 disease phenotypes and genotypes associated with mutations in presenilin 2. Brain.
797 2010;133(Pt 4):1143-54.
798 5. Kang DE, Yoon IS, Repetto E, Busse T, Yermian N, Ie L, et al. Presenilins mediate
799 phosphatidylinositol 3-kinase/AKT and ERK activation via select signaling
800 receptors. Selectivity of PS2 in platelet-derived growth factor signaling. J Biol
801 Chem. 2005;280(36):31537-47.
802 6. Lee MK, Slunt HH, Martin LJ, Thinakaran G, Kim G, Gandy SE, et al. Expression
803 of presenilin 1 and 2 (PS1 and PS2) in human and murine tissues. J Neurosci.
804 1996;16(23):7513-25.
805 7. Jiang H, Jayadev S, Lardelli M, Newman M. A Review of the Familial Alzheimer's
806 Disease Locus PRESENILIN 2 and Its Relationship to PRESENILIN 1. Journal of

807 Alzheimer's disease : JAD. 2018;66(4):1323-39.

808 8. De Strooper B, Saftig P, Craessaerts K, Vanderstichele H, Guhde G, Annaert W,
809 et al. Deficiency of presenilin-1 inhibits the normal cleavage of amyloid precursor
810 protein. Nature. 1998;391(6665):387-90.

811 9. Naruse S, Thinakaran G, Luo JJ, Kusiak JW, Tomita T, Iwatsubo T, et al. Effects
812 of PS1 deficiency on membrane protein trafficking in neurons. Neuron.
813 1998;21(5):1213-21.

814 10. Herreman A, Serneels L, Annaert W, Collen D, Schoonjans L, De Strooper B. Total
815 inactivation of gamma-secretase activity in presenilin-deficient embryonic stem
816 cells. Nature cell biology. 2000;2(7):461-2.

817 11. Zhang Z, Nadeau P, Song W, Donoviel D, Yuan M, Bernstein A, et al. Presenilins
818 are required for gamma-secretase cleavage of beta-APP and transmembrane
819 cleavage of Notch-1. Nat Cell Biol. 2000;2(7):463-5.

820 12. Jayne T, Newman M, Verdile G, Sutherland G, Munch G, Musgrave I, et al.
821 Evidence For and Against a Pathogenic Role of Reduced gamma-Secretase
822 Activity in Familial Alzheimer's Disease. Journal of Alzheimer's disease : JAD.
823 2016;52(3):781-99.

824 13. Shen J, Bronson RT, Chen DF, Xia W, Selkoe DJ, Tonegawa S. Skeletal and CNS
825 defects in Presenilin-1-deficient mice. Cell. 1997;89(4):629-39.

826 14. Handler M, Yang X, Shen J. Presenilin-1 regulates neuronal differentiation during
827 neurogenesis. Development. 2000;127(12):2593-606.

828 15. Ferjentsik Z, Hayashi S, Dale JK, Bessho Y, Herreman A, De Strooper B, et al.

829 Notch Is a Critical Component of the Mouse Somitogenesis Oscillator and Is
830 Essential for the Formation of the Somites. PLOS Genetics. 2009;5(9):e1000662.
831 16. Donoviel DB, Hadjantonakis AK, Ikeda M, Zheng H, Hyslop PS, Bernstein A.
832 Mice lacking both presenilin genes exhibit early embryonic patterning defects.
833 Genes Dev. 1999;13(21):2801-10.
834 17. Herreman A, Hartmann D, Annaert W, Saftig P, Craessaerts K, Serneels L, et al.
835 Presenilin 2 deficiency causes a mild pulmonary phenotype and no changes in
836 amyloid precursor protein processing but enhances the embryonic lethal phenotype
837 of presenilin 1 deficiency. Proceedings of the National Academy of Sciences.
838 1999;96(21):11872-7.
839 18. Nornes S, Newman M, Verdile G, Wells S, Stoick-Cooper CL, Tucker B, et al.
840 Interference with splicing of Presenilin transcripts has potent dominant negative
841 effects on Presenilin activity. Human molecular genetics. 2008;17(3):402-12.
842 19. Wang P, Pereira FA, Beasley D, Zheng H. Presenilins are required for the
843 formation of comma- and S-shaped bodies during nephrogenesis. Development.
844 2003;130(20):5019-29.
845 20. Jayadev S, Case A, Eastman AJ, Nguyen H, Pollak J, Wiley JC, et al. Presenilin 2
846 is the predominant gamma-secretase in microglia and modulates cytokine release.
847 PLoS ONE. 2010;5(12):0015743.
848 21. Jayadev S, Case A, Alajajian B, Eastman AJ, Möller T, Garden GA. Presenilin 2
849 influences miR146 level and activity in microglia. Journal of Neurochemistry.
850 2013;127(5):592-9.

851 22. Agrawal V, Sawhney N, Hickey E, McCarthy JV. Loss of Presenilin 2 Function Is
852 Associated with Defective LPS-Mediated Innate Immune Responsiveness.
853 Molecular Neurobiology. 2016;53(5):3428-38.
854 23. Area-Gomez E, de Groof AJ, Boldogh I, Bird TD, Gibson GE, Koehler CM, et al.
855 Presenilins are enriched in endoplasmic reticulum membranes associated with
856 mitochondria. The American journal of pathology. 2009;175(5):1810-6.
857 24. Marchi S, Patergnani S, Pinton P. The endoplasmic reticulum–mitochondria
858 connection: One touch, multiple functions. Biochimica et Biophysica Acta (BBA)
859 - Bioenergetics. 2014;1837(4):461-9.
860 25. Behbahani H, Shabalina IG, Wiehager B, Concha H, Hultenby K, Petrovic N, et al.
861 Differential role of Presenilin-1 and -2 on mitochondrial membrane potential and
862 oxygen consumption in mouse embryonic fibroblasts. J Neurosci Res.
863 2006;84(4):891-902.
864 26. Hroudova J, Singh N, Fisar Z. Mitochondrial dysfunctions in neurodegenerative
865 diseases: relevance to Alzheimer's disease. Biomed Res Int. 2014;175062(10):12.
866 27. Zampese E, Fasolato C, Kipanyula MJ, Bortolozzi M, Pozzan T, Pizzo P. Presenilin
867 2 modulates endoplasmic reticulum (ER)-mitochondria interactions and Ca2+
868 cross-talk. Proc Natl Acad Sci U S A. 2011;108(7):2777-82.
869 28. Contino S, Porporato PE, Bird M, Marinangeli C, Opsomer R, Sonveaux P, et al.
870 Presenilin 2-Dependent Maintenance of Mitochondrial Oxidative Capacity and
871 Morphology. Front Physiol. 2017;8(796).
872 29. Hwang WY, Fu Y, Reyon D, Maeder ML, Tsai SQ, Sander JD, et al. Efficient

873 genome editing in zebrafish using a CRISPR-Cas system. Nat Biotechnol.
874 2013;31(3):227-9.
875 30. Babon JJ, McKenzie M, Cotton RGH. The use of resolvases T4 endonuclease VII
876 and T7 endonuclease I in mutation detection. Molecular Biotechnology.
877 2003;23(1):73-81.
878 31. Meeker ND, Hutchinson SA, Ho L, Trede NS. Method for isolation of PCR-ready
879 genomic DNA from zebrafish tissues. Biotechniques. 2007;43(5):614.
880 32. Adiconis X, Borges-Rivera D, Satija R, DeLuca DS, Busby MA, Berlin AM, et al.
881 Comparative analysis of RNA sequencing methods for degraded or low-input
882 samples. Nat Methods. 2013;10(7):623-9.
883 33. Dobin A, Davis CA, Schlesinger F, Drenkow J, Zaleski C, Jha S, et al. STAR:
884 ultrafast universal RNA-seq aligner. Bioinformatics. 2013;29(1):15-21.
885 34. Bray NL, Pimentel H, Melsted P, Pachter L. Near-optimal probabilistic RNA-seq
886 quantification. Nat Biotechnol. 2016;34(5):525-7.
887 35. Liao Y, Smyth GK, Shi W. The Subread aligner: fast, accurate and scalable read
888 mapping by seed-and-vote. Nucleic Acids Research. 2013;41(10):e108-e.
889 36. Hansen KD, Irizarry RA, Wu Z. Removing technical variability in RNA-seq data
890 using conditional quantile normalization. Biostatistics. 2012;13(2):204-16.
891 37. Robinson MD, McCarthy DJ, Smyth GK. edgeR: a Bioconductor package for
892 differential expression analysis of digital gene expression data. Bioinformatics.
893 2010;26(1):139-40.
894 38. Liberzon A. A description of the Molecular Signatures Database (MSigDB) Web

895 site. Methods Mol Biol. 2014;1150:153-60.

896 39. Young MD, Wakefield MJ, Smyth GK, Oshlack A. Gene ontology analysis for
897 RNA-seq: accounting for selection bias. Genome Biol. 2010;11(2):R14.

898 40. Wu D, Lim E, Vaillant F, Asselin-Labat ML, Visvader JE, Smyth GK. ROAST:
899 rotation gene set tests for complex microarray experiments. Bioinformatics.
900 2010;26(17):2176-82.

901 41. Nornes S, Newman M, Wells S, Verdile G, Martins RN, Lardelli M. Independent
902 and cooperative action of Psen2 with Psen1 in zebrafish embryos. Experimental
903 Cell Research. 2009;315(16):2791-801.

904 42. Groth C, Nornes S, McCarty R, Tamme R, Lardelli M. Identification of a second
905 presenilin gene in zebrafish with similarity to the human Alzheimer's disease gene
906 presenilin2. Dev Genes Evol. 2002;212(10):486-90.

907 43. Brogna S, Wen J. Nonsense-mediated mRNA decay (NMD) mechanisms. Nat
908 Struct Mol Biol. 2009;16(2):107-13.

909 44. Zetterberg H, Mortberg E, Song L, Chang L, Provuncher GK, Patel PP, et al.
910 Hypoxia due to cardiac arrest induces a time-dependent increase in serum amyloid
911 beta levels in humans. PLoS ONE. 2011;6(12):14.

912 45. Gao L, Tian S, Gao H, Xu Y. Hypoxia increases Abeta-induced tau
913 phosphorylation by calpain and promotes behavioral consequences in AD
914 transgenic mice. J Mol Neurosci. 2013;51(1):138-47.

915 46. Mohuczy D, Qian K, Phillips MI. Presenilins in the heart: presenilin-2 expression
916 is increased by low glucose and by hypoxia in cardiac cells. Regul Pept.

2002;110(1):1-7.

47. Ebrahimie E, Moussavi Nik SH, Newman M, Van Der Hoek M, Lardelli M. The Zebrafish Equivalent of Alzheimer's Disease-Associated PRESENILIN Isoform PS2V Regulates Inflammatory and Other Responses to Hypoxic Stress. Journal of Alzheimer's disease : JAD. 2016;52(2):581-608.

48. Jiang H, Newman M, Lardelli M. The zebrafish orthologue of familial Alzheimer's disease gene PRESENILIN 2 is required for normal adult melanotic skin pigmentation. PloS one. 2018;13(10):e0206155.

49. Rossi A, Kontarakis Z, Gerri C, Nolte H, Hölper S, Krüger M, et al. Genetic compensation induced by deleterious mutations but not gene knockdowns. Nature. 2015;524:230.

50. Tamme R, Wells S, Conran JG, Lardelli M. The identity and distribution of neural cells expressing the mesodermal determinant spadetail. BMC Developmental Biology. 2002;2(1):9.

51. Schiffer NW, Broadley SA, Hirschberger T, Tavan P, Kretzschmar HA, Giese A, et al. Identification of anti-prion compounds as efficient inhibitors of polyglutamine protein aggregation in a zebrafish model. The Journal of biological chemistry. 2007;282(12):9195-203.

52. Ni HM, Bockus A, Wozniak AL, Jones K, Weinman S, Yin XM, et al. Dissecting the dynamic turnover of GFP-LC3 in the autolysosome. Autophagy. 2011;7(2):188-204.

53. Mandelboum S, Manber Z, Elroy-Stein O, Elkon R. Recurrent functional

939 misinterpretation of RNA-seq data caused by sample-specific gene length bias.
940 PLoS Biol. 2019;17(11):e3000481.
941 54. Newman M, Hin N, Pederson S, Lardelli M. Brain transcriptome analysis of a
942 familial Alzheimer's disease-like mutation in the zebrafish presenilin 1 gene
943 implies effects on energy production. Molecular Brain. 2019.
944 55. Nagy E, Maquat LE. A rule for termination-codon position within intron-
945 containing genes: when nonsense affects RNA abundance. Trends in biochemical
946 sciences. 1998;23(6):198-9.
947 56. Area-Gomez E, Del Carmen Lara Castillo M, Tambini MD, Guardia-Laguarta C,
948 de Groof AJ, Madra M, et al. Upregulated function of mitochondria-associated ER
949 membranes in Alzheimer disease. The EMBO journal. 2012;31(21):4106-23.
950 57. Pera M, Larrea D, Guardia-Laguarta C, Montesinos J, Velasco KR, Agrawal RR,
951 et al. Increased localization of APP-C99 in mitochondria-associated ER
952 membranes causes mitochondrial dysfunction in Alzheimer disease. The EMBO
953 journal. 2017;36(22):3356-71.
954 58. Lee JH, Yu WH, Kumar A, Lee S, Mohan PS, Peterhoff CM, et al. Lysosomal
955 proteolysis and autophagy require presenilin 1 and are disrupted by Alzheimer-
956 related PS1 mutations. Cell. 2010;141(7):1146-58.
957 59. Yambire KF, Rostosky C, Watanabe T, Pacheu-Grau D, Torres-Odio S, Sanchez-
958 Guerrero A, et al. Impaired lysosomal acidification triggers iron deficiency and
959 inflammation in vivo. Elife. 2019;8.
960 60. Jiang Y, Sato Y, Im E, Berg M, Bordi M, Darji S, et al. Lysosomal Dysfunction in

961 Down Syndrome Is APP-Dependent and Mediated by APP-betaCTF (C99). The
962 Journal of neuroscience : the official journal of the Society for Neuroscience.
963 2019;39(27):5255-68.

964

965

Supporting information

Supplementary data files:

S1 Appendix 1. ***psen2*-EGFP fusion gene sequences**

S1 Table 1. **Expression levels of the wild type *psen2* allele in 25ng total adult brain cDNA**

S1 Table 2. **Expression levels of the *psen2*^{S4Ter} allele in 25ng total adult brain cDNA**

S1 Table 3. **Numbers of DoLA neurons in 24 hpf embryos (revealed by *in situ* transcript hybridization against *tbx16* mRNA)**

S1 Appendix 2. ***psen2*^{S4Ter} transcript splicing tests**

S2 Sheet 1. **DE genes – presence of S4Ter mutation vs. wild type**

S2 Sheet 2. **Pathway enrichment – presence of S4Ter mutation vs. wild type**

S2 Sheet 3. **DE genes – S4Ter Hom vs. S4Ter Het.**

S2. Sheet 4. **Pathway enrichment – S4Ter Hom vs. S4Ter Het.**

A **Genes differentially expressed due to presence of *psen2*^{S4Ter} allele**

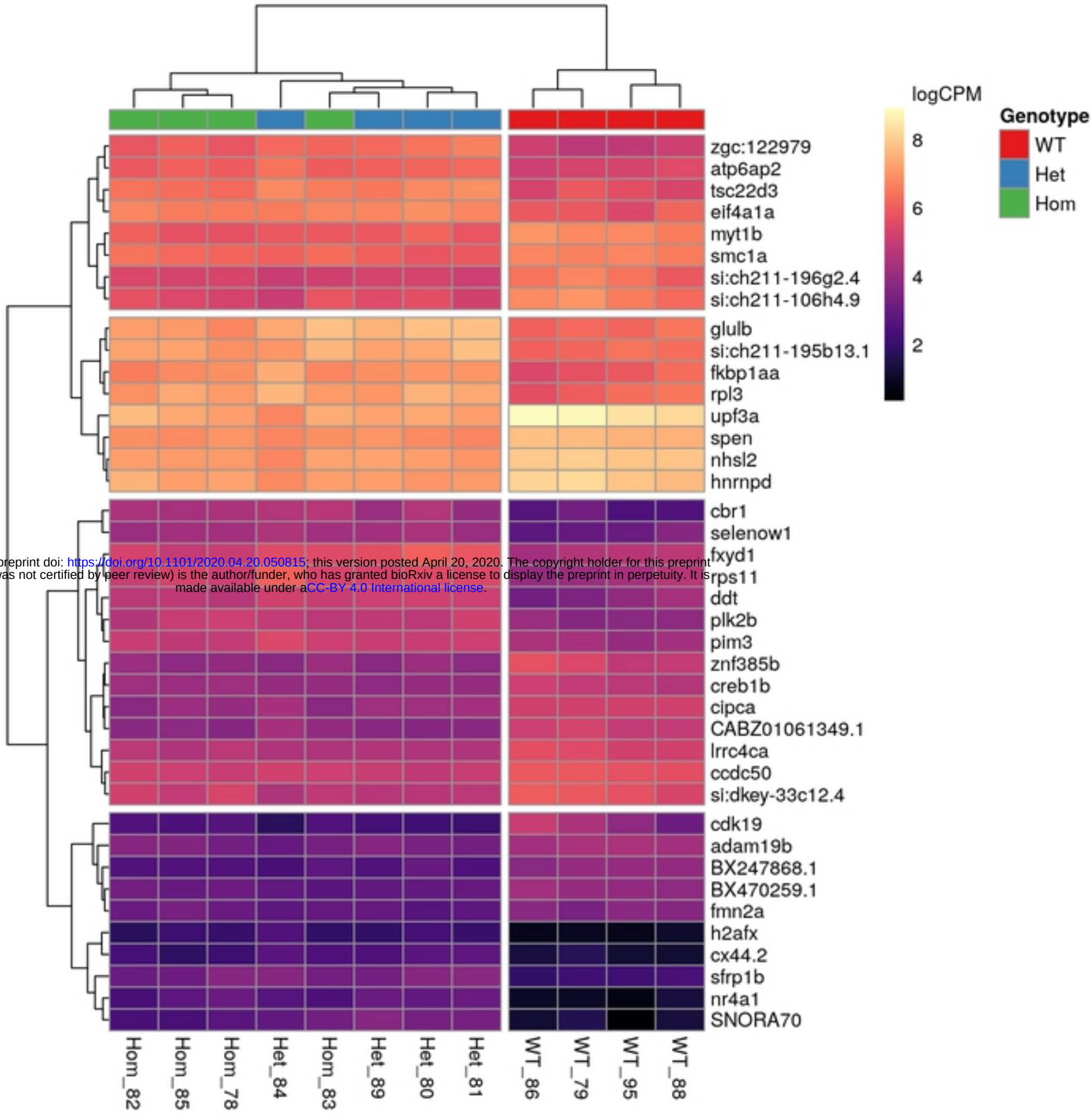

B **Genes differentially expressed between Het and Hom genotypes**

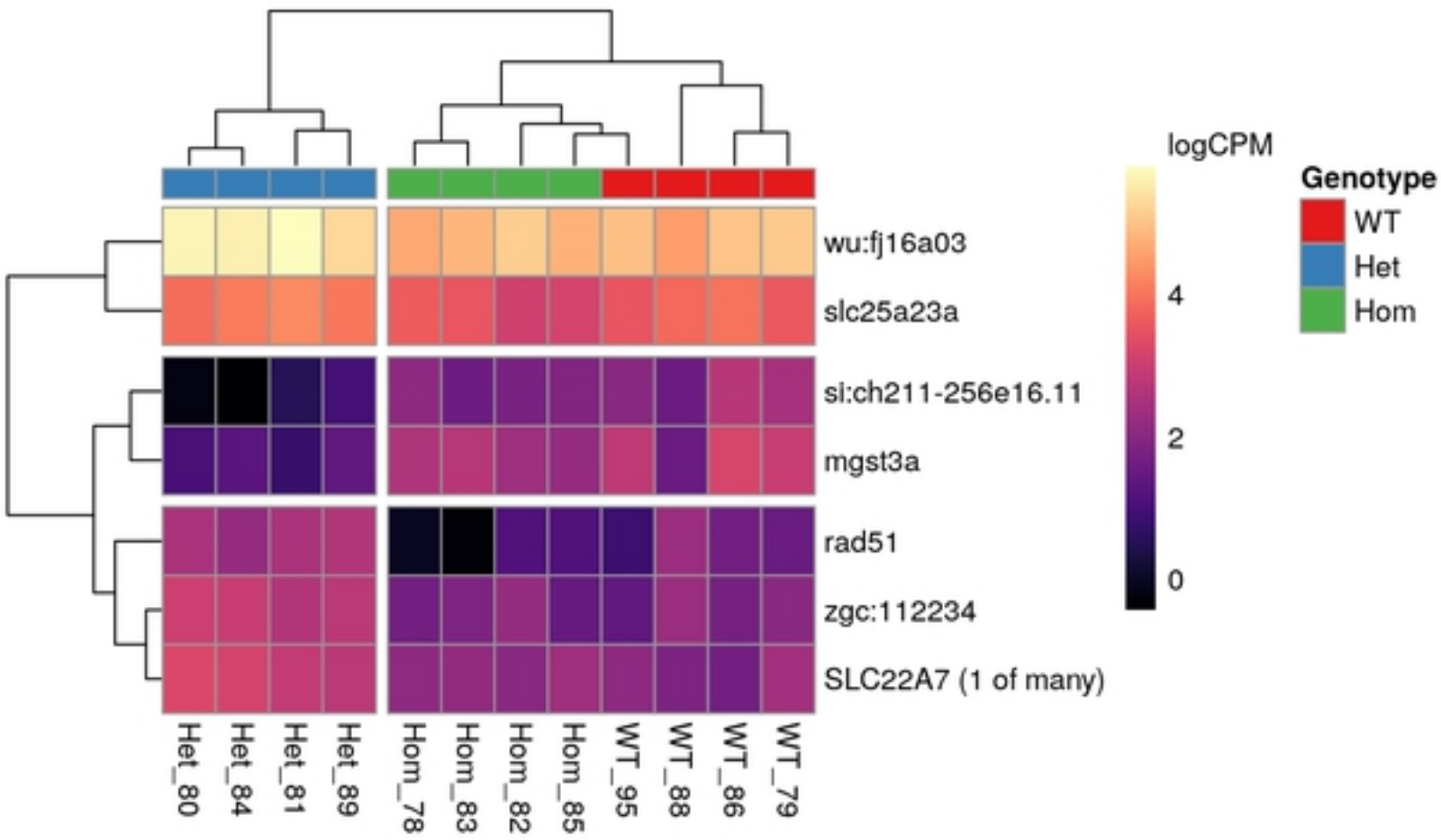

Figure 6

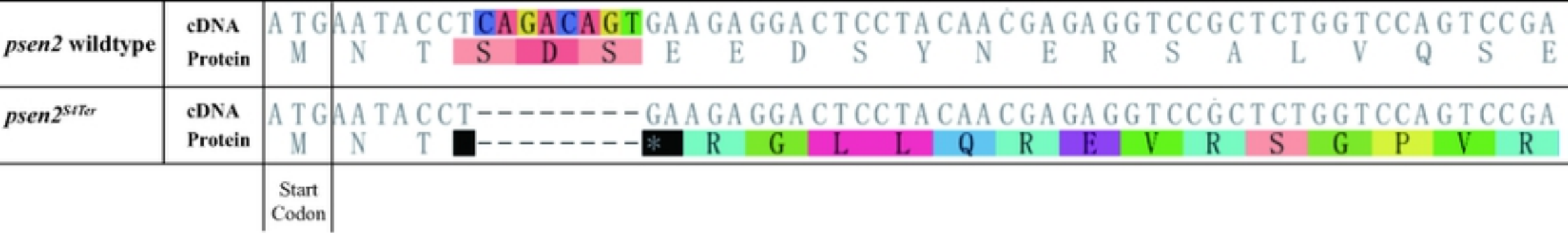
psen2 wildtype
cDNA
Protein
ATGAATACCTCAGACAGTGAAGAGGACTCCTACAACGAGAGGTCCGCTCTGGTCCAGTCCGA
M N T S D S E E D S Y N E R S A L V Q S E
psen2StTer
cDNA
Protein
ATGAATACCT---------GAAGAGGACTCCTACAACGAGAGGTCCGCTCTGGTCCAGTCCGA
M N T ■---------* R G L L Q R E V R S G P V R
Start Codon

Figure 1

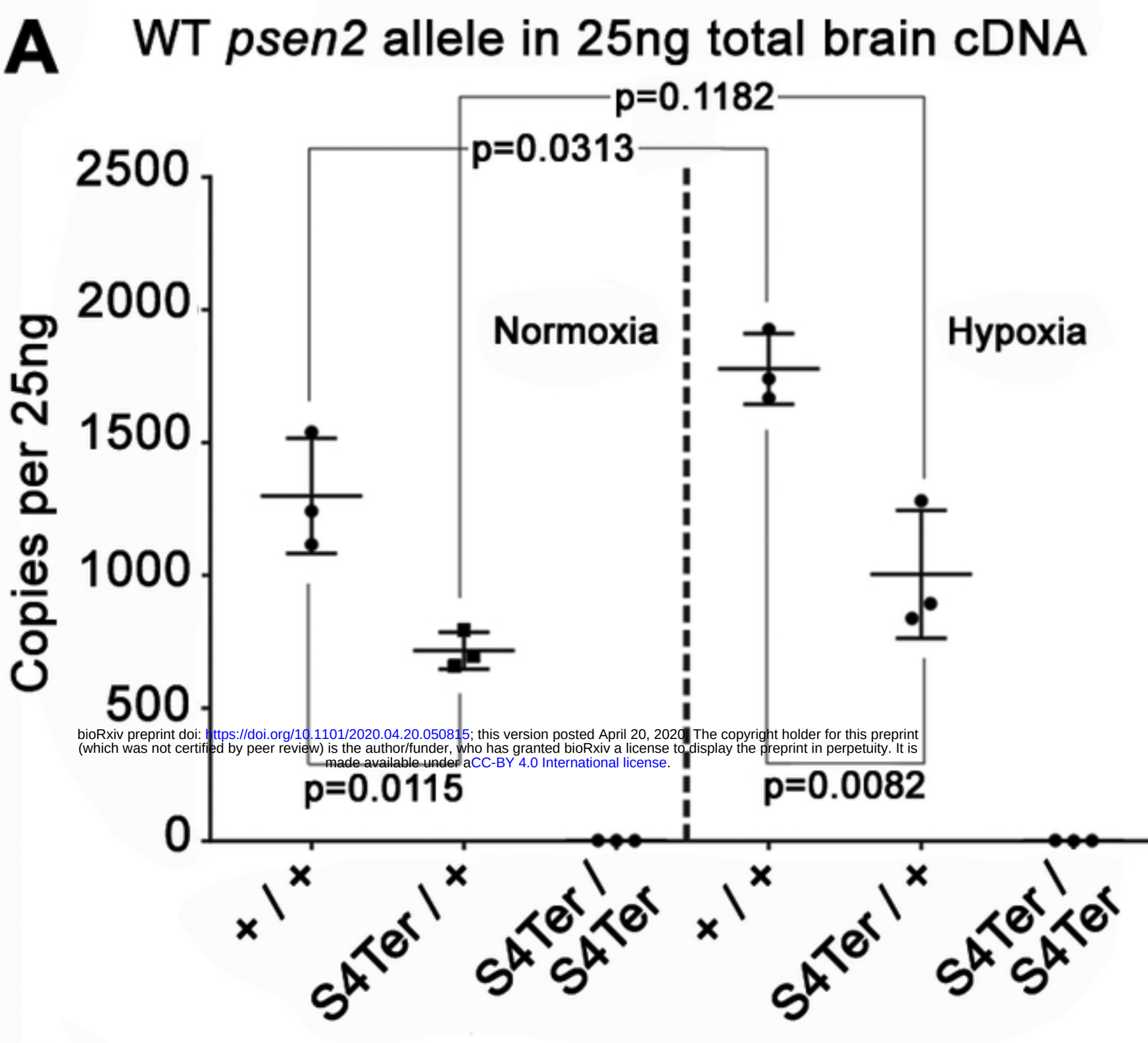

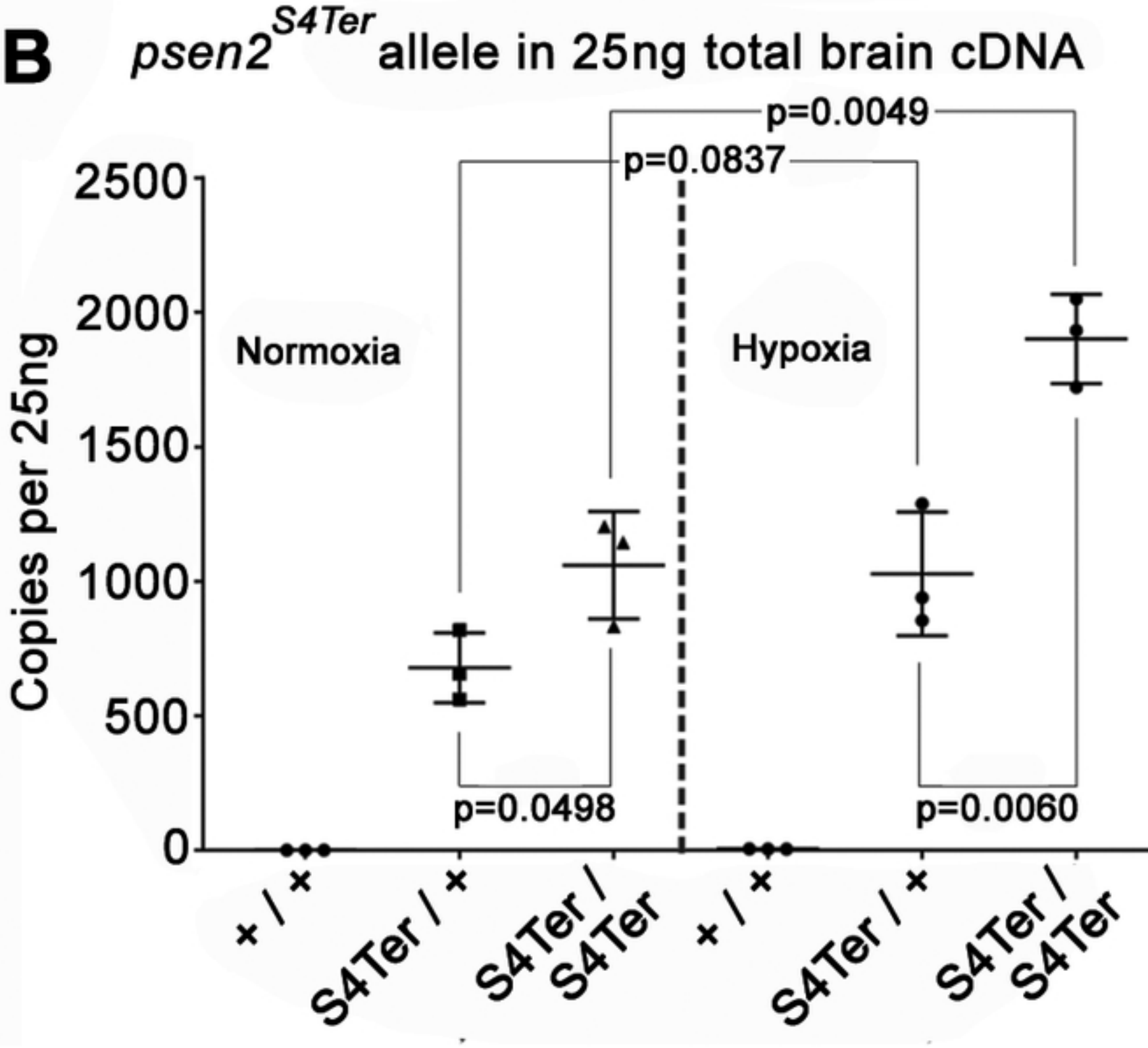

Figure 2

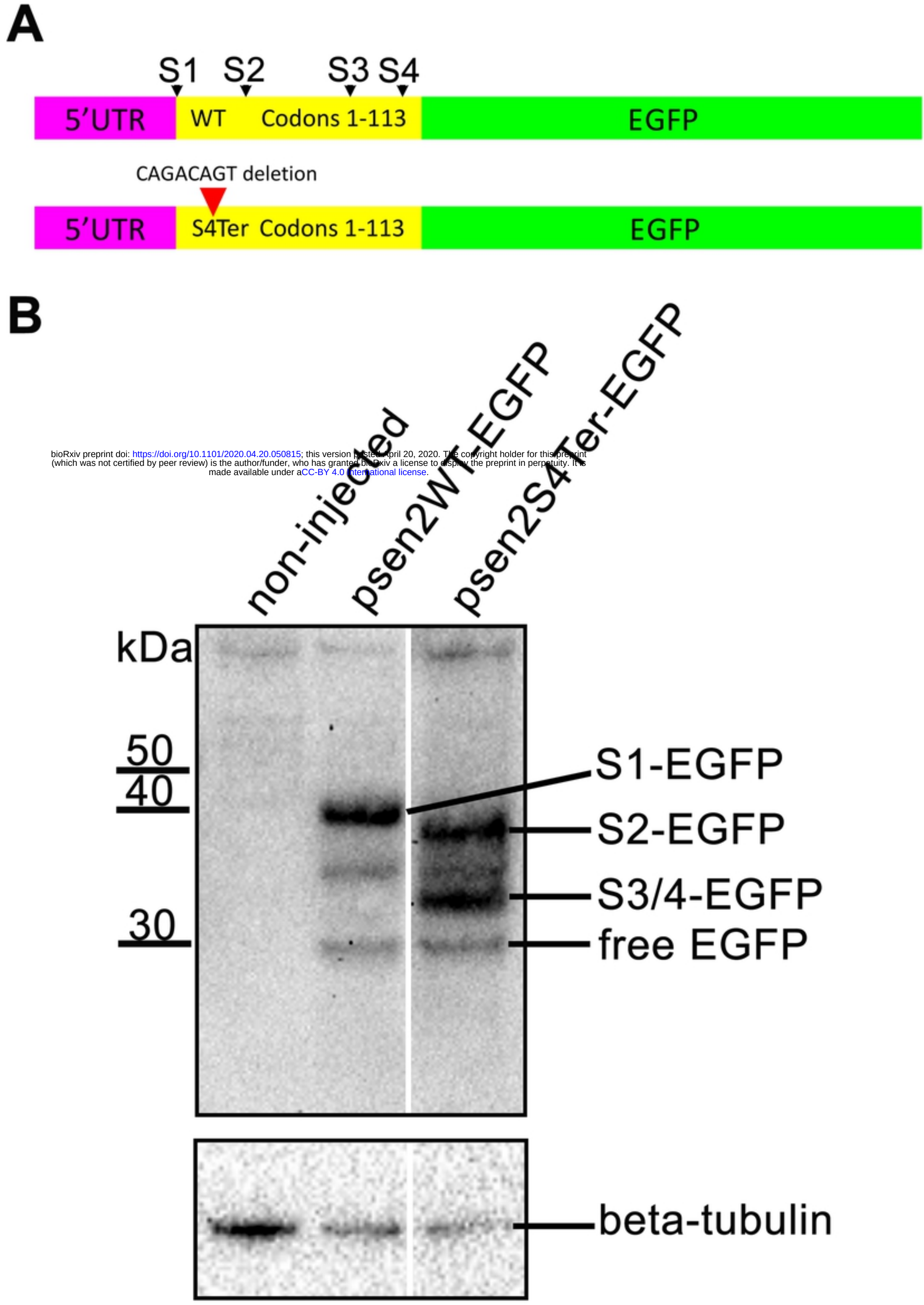

Figure 4

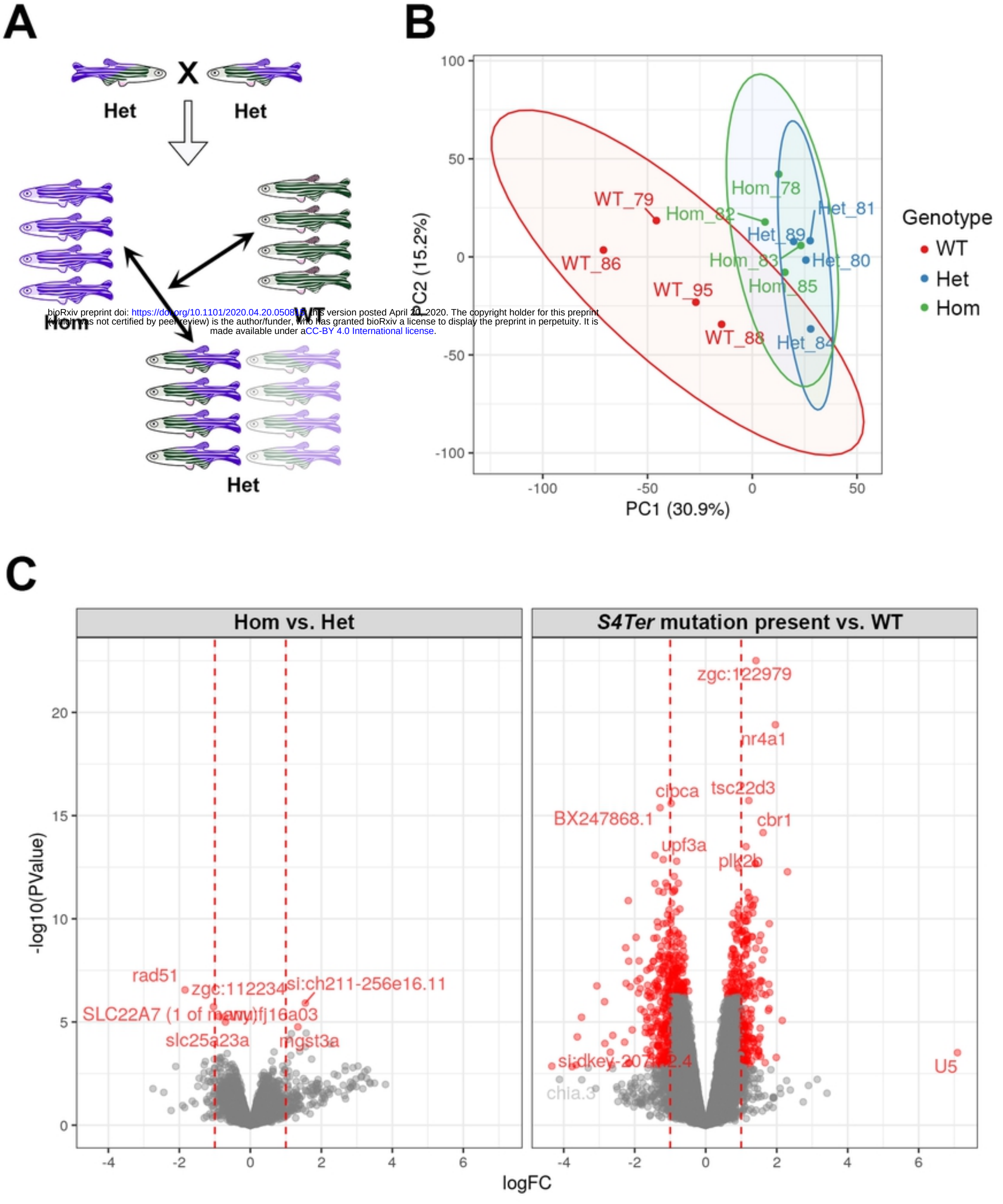

Figure 5

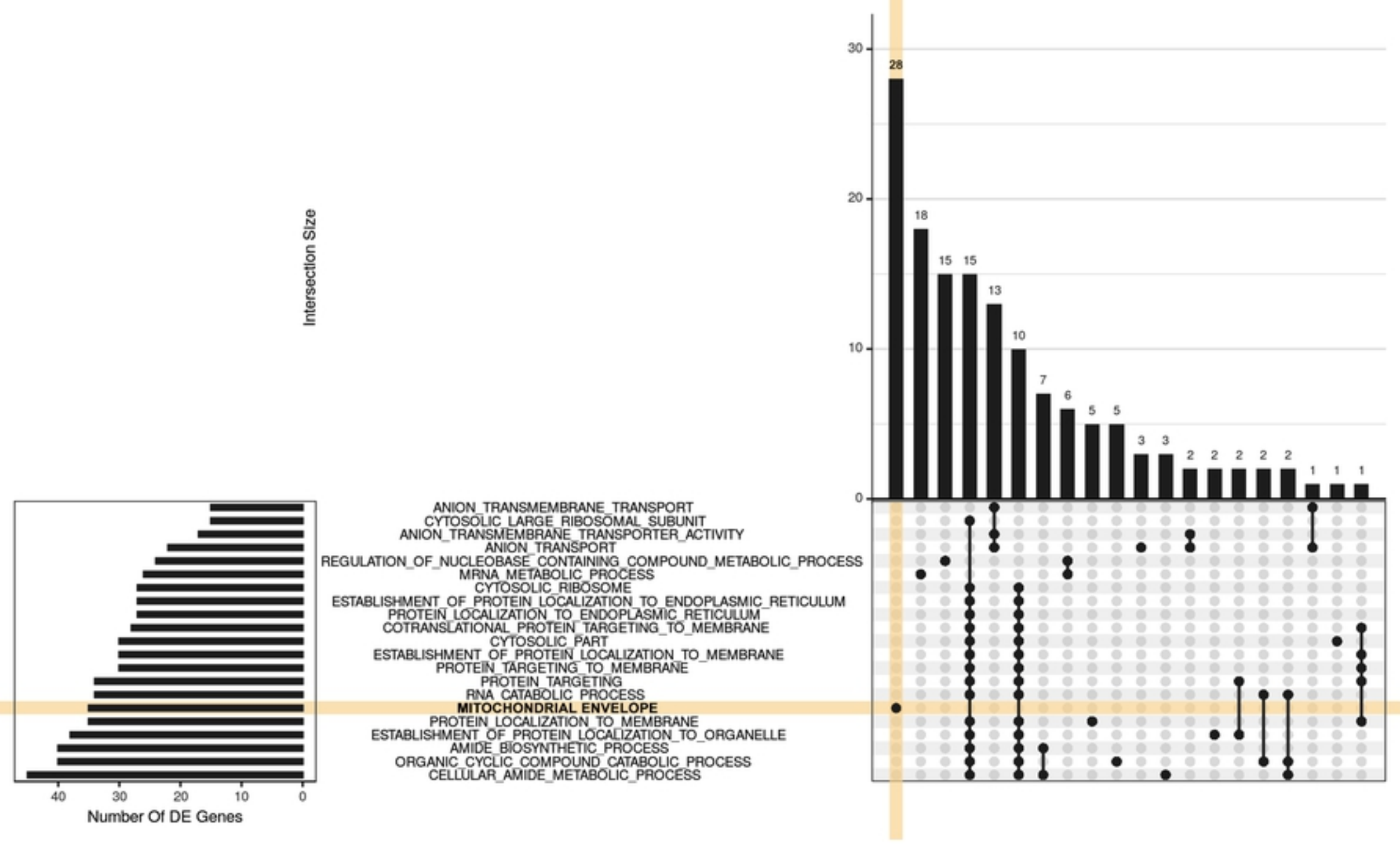
Intersection Size
30
20
10
0
28
18
15
15
13
10
7
6
5
5
3
3
2
2
2
2
2
1
1
1
ANION_TRANSMEMBRANE_TRANSPORT
CYTOSOLIC_LARGE_RIBOSOMAL_SUBUNIT
ANION_TRANSMEMBRANE_TRANSPORTER_ACTIVITY
ANION_TRANSPORT
REGULATION_OF_NUCLEOBASE_CONTAINING_COMPOUND_METABOLIC_PROCESS
MRNA_METABOLIC_PROCESS
CYTOSOLIC_RIBOSOME
ESTABLISHMENT_OF_PROTEIN_LOCALIZATION_TO_ENDOPLASMIC_RETICULUM
PROTEIN_LOCALIZATION_TO_ENDOPLASMIC_RETICULUM
COTRANSLATIONAL_PROTEIN_TARGETING_TO_MEMBRANE
CYTOSOLIC_PART
ESTABLISHMENT_OF_PROTEIN_LOCALIZATION_TO_MEMBRANE
PROTEIN_TARGETING_TO_MEMBRANE
PROTEIN_TARGETING
RNA_CATABOLIC_PROCESS
MITOCHONDRIAL ENVELOPE
PROTEIN_LOCALIZATION_TO_MEMBRANE
ESTABLISHMENT_OF_PROTEIN_LOCALIZATION_TO_ORGANELLE
AMIDE_BIOSYNTHETIC_PROCESS
ORGANIC_CYCLIC_COMPOUND_CATABOLIC_PROCESS
CELLULAR_AMIDE_METABOLIC_PROCESS
40
30
20
10
0
Number Of DE Genes

Figure 7

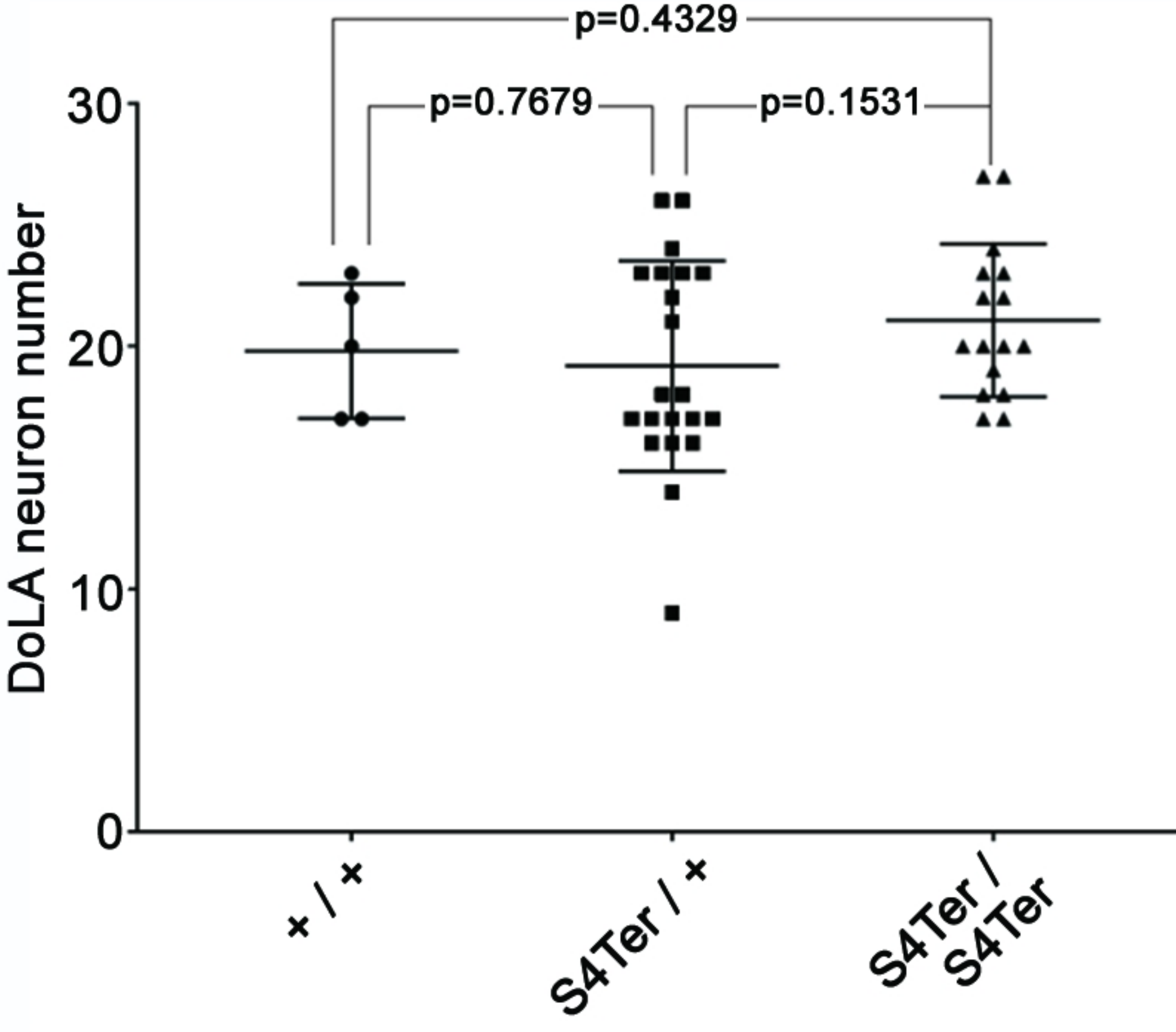
p=0.4329
p=0.7679
p=0.1531
30
20
10
0
DoLA neuron number
+ / +
S4Ter / +
S4Ter / S4Ter

Figure 3